SPECIAL FEATURE: PERSPECTIVE

Neogene biomarker record of vegetation change in eastern Africa

Kevin T. Uno[a,1], Pratigya J. Polissar[a], Kevin E. Jackson[b], and Peter B. deMenocal[a,c]

Edited by Richard G. Klein, Stanford University, Stanford, CA, and approved April 26, 2016 (received for review February 1, 2016)

The evolution of C_4 grassland ecosystems in eastern Africa has been intensely studied because of the potential influence of vegetation on mammalian evolution, including that of our own lineage, hominins. Although a handful of sparse vegetation records exists from middle and early Miocene terrestrial fossil sites, there is no comprehensive record of vegetation through the Neogene. Here we present a vegetation record spanning the Neogene and Quaternary Periods that documents the appearance and subsequent expansion of C_4 grasslands in eastern Africa. Carbon isotope ratios from terrestrial plant wax biomarkers deposited in marine sediments indicate constant C_3 vegetation from ∼24 Ma to 10 Ma, when C_4 grasses first appeared. From this time forward, C_4 vegetation increases monotonically to present, with a coherent signal between marine core sites located in the Somali Basin and the Red Sea. The response of mammalian herbivores to the appearance of C_4 grasses at 10 Ma is immediate, as evidenced from existing records of mammalian diets from isotopic analyses of tooth enamel. The expansion of C_4 vegetation in eastern Africa is broadly mirrored by increasing proportions of C_4-based foods in hominin diets, beginning at 3.8 Ma in *Australopithecus* and, slightly later, *Kenyanthropus*. This continues into the late Pleistocene in *Paranthropus*, whereas *Homo* maintains a flexible diet. The biomarker vegetation record suggests the increase in open, C_4 grassland ecosystems over the last 10 Ma may have operated as a selection pressure for traits and behaviors in *Homo* such as bipedalism, flexible diets, and complex social structure.

leaf wax | carbon isotope | mammalian evolution | molecular distribution | hominin

One of the central questions in human evolution is what role, if any, did climate play in shaping who we are? Climate largely determines the types of vegetation that can grow in a given ecosystem and thus defines the plant foods and habitat available to fauna in that ecosystem. Therefore, if climate-driven vegetation changes occurred during important transitions in the evolution of humans, it could indicate that climate influenced the evolution of our ancestors. Within this framework, paleovegetation records can be used to evaluate how climate-driven vegetation changes affected mammalian evolutionary events, such as changes in dietary or faunal composition, at a variety of spatial and temporal scales. We give a concise summary of the results from paleovegetation proxies applied in eastern Africa to date and we present new results from carbon isotope data from terrestrial plant waxes representing a broad spatial and temporal scale.

The story of human evolution has largely unfolded in eastern Africa during the Neogene. Our lineage, the hominins, first appeared in the late Miocene or early Pliocene after splitting from chimpanzees between 7 Ma and 5 Ma based on molecular divergence rates (1, 2). In the past few decades, new discoveries have greatly expanded the number of hominins in the fossil record, and, in concert, new paleoenvironmental records (3–8) and syntheses (9–11) have expanded our understanding of hominin paleoenvironments in eastern Africa. The set of tools available for studying paleovegetation has also expanded considerably, and a diverse series of approaches are being used in eastern Africa.

Neogene Vegetation Change in Eastern Africa

Paleobotanical remains from macrofossils (leaves, stems, roots, seeds, nuts, etc.) and microfossils (pollen and phytoliths) are direct evidence of vegetation in ancient environments. Plant macrofossils provide key information for vegetation reconstructions at Neogene fossil sites in Ethiopia, Kenya, Tanzania, and Uganda (6, 12–20). Collectively, the sites indicate wooded habitats ranging from wet forests (17), some with understory bamboo grasses (15), to closed canopy forests (20), to woodlands (18, 19). However, with rare exception (6, 12–14) plant macrofossils are absent from the more

[a]Lamont-Doherty Earth Observatory of Columbia University, Palisades, NY 10964; [b]Department of Geology and Environmental Geosciences, Lafayette College, Easton, PA 18042; and [c]Department of Earth and Environmental Sciences, Columbia University, New York, NY 10027

Author contributions: K.T.U., P.J.P., and P.B.d. designed research; K.T.U., P.J.P., and K.E.J. performed research; P.J.P. contributed new reagents/analytic tools; K.T.U., P.J.P., K.E.J., and P.B.d. analyzed data; and K.T.U. wrote the paper with input from all coauthors.

The authors declare no conflict of interest.

This article is a PNAS Direct Submission.

[1]To whom correspondence should be addressed. Email: kevinuno1@gmail.com.

This article contains supporting information online at www.pnas.org/lookup/suppl/doi:10.1073/pnas.1521267113/-/DCSupplemental.

stratigraphically continuous latest Miocene to Pleistocene sites in eastern Africa.

Pollen and phytolith records from floodplain sediments, paleosols, or lakes (21–23) reflect local vegetation, whereas distal records, such as those from marine cores, represent regional vegetation (9, 24) and are subject to greater dispersal bias (25). In eastern Africa, Raymonde Bonnefille's perseverance in extracting pollen from seemingly unpromising terrestrial sediments has yielded vegetation reconstructions at numerous Plio-Pleistocene hominin sites (22, 23, 26, 27). The pollen data illustrate that, within the shift toward more arid conditions over the past ∼5 My, vegetation at individual sites remained highly variable through time and, at any given time interval, there was heterogeneity between sites.

Phytoliths are microscopic opaline silica bodies with taxonomically diagnostic morphologies (28). Their presence in the geologic record is powerful because of their greater resistance to degradation than pollen under oxidative conditions and, critically, because of their ability to distinguish C_3 and C_4 grasses apart from one another (29). Increasingly, phytoliths are being used to reconstruct Miocene to Pleistocene ecosystems in Africa (5, 14, 29, 30).

Another perspective on hominin paleoenvironments comes from carbon isotope analysis. Plants using the Calvin cycle, or C_3 photosynthetic pathway, including trees, shrubs, forbs, and cool season grasses, have more negative carbon isotope values, whereas plants using the Hatch–Slack cycle, or C_4 pathway, including warm season grasses and sedges, have more positive carbon isotope values (31). In eastern Africa today, the carbon isotope ratio of plants can be used to discriminate between grassy and woody vegetation because nearly all grasses below 3,000 m use the C_4 pathway, whereas nearly all woody vegetation uses the C_3 pathway (32, 33). Direct reconstruction of vegetation in eastern Africa using carbon isotopes comes almost exclusively from pedogenic carbonate, which, when formed in equilibrium with soil CO_2, reflects the proportion of C_3 to C_4 vegetation in past landscapes (34, 35). Carbon isotope data from pedogenic carbonate have contributed substantially to our understanding of vegetation at Miocene to Pleistocene hominid fossil sites (ref. 4 and references therein).

Carbon isotope data from fossil tooth enamel have been fundamental to understanding dietary changes in large mammals in eastern Africa (e.g., refs. 36 and 37) and, more broadly, paleoenvironments at eastern African fossil sites. The carbon isotope ratio of fossil enamel reflects the proportion of C_3 and C_4 vegetation in the diets of mammals (38–40). Large isotope data sets representative of mammalian fauna provide important information about the relative contributions of C_3 and C_4 biomass on the landscape (e.g., refs. 41–43), although the dietary information does not directly reflect quantitative vegetation distributions.

Another carbon isotope archive for reconstructing eastern African paleovegetation that has emerged as a powerful tool in the past decade is terrestrial plant waxes from sediments (7, 8, 44). Plant wax biomarkers derive primarily from epicuticular leaf waxes that protect the leaf tissue from abrasion by dust; attack from insects, microbes, and fungi; and water loss from the leaf surface. The waxes are primarily long chain, linear or normal (*n*-)alkyl lipids made up of carbon and hydrogen atoms (45). Terrestrial plant waxes are commonly transported via fluvial and aeolian processes and are preserved in terrestrial and marine sediments (46–48). Marine sediments typically accumulate slowly and continuously and can be well dated. Thus, terrestrial plant waxes from marine sediments serve as useful archives of regional vegetation change (49), making them an excellent complement to terrestrial sedimentary deposits. Paleovegetation records from terrestrial sediments are biased toward lowland vegetation simply because sediment accumulation occurs in basins. Thus, carbon isotopes in plant waxes from terrestrial sites provide a local vegetation signal (44), whereas waxes from marine sediments provide a regionally integrated signal.

Beyond elucidating the paleoenvironments and diets of eastern African fauna, carbon isotope data from pedogenic carbonates, fossil enamel, and plant waxes, were critical in the discovery of the global expansion of C_4 grasslands in the late Miocene (see review in ref. 50). This includes pedogenic carbonate records from the Siwaliks (51–53), North America (54), and Africa (52, 55). Tooth enamel data were also used to document the rise of grasslands between 8 Ma and 5 Ma in these same regions (56–58). More recently, carbon isotope records from plant waxes in the Siwaliks (48), North America (49), and eastern Africa (7) have further characterized this global ecological transition. Several of these isotopic records indicate minor amounts of C_4 vegetation in the middle Miocene of North America (49, 54) and possibly in eastern Africa (52). Plant wax (7) and more recent tooth enamel data (36, 59) suggest the rise of C_4 grasses in eastern Africa was earlier than in other parts of the world, yet there is no continuous vegetation record from the Neogene, and data before 10 Ma are sparse.

Characterizing the timing and nature of the C_4 grassland expansion and evaluating its potential role in the evolution of mammals and humans in eastern Africa requires a regional, full Neogene record of vegetation. The patchy and discontinuous distribution of early and middle Miocene fossil sites in eastern Africa precludes terrestrial sediments from providing such a record. Marine sediments, on the other hand, offer the opportunity to produce a long, continuous, regionally representative vegetation record from the Neogene to present. A series of Deep Sea Drilling Project (DSDP) cores proximal to eastern Africa were recovered from the Somali Basin (western Indian Ocean), the Red Sea, and the Gulf of Aden in the early 1970s. One of these cores, DSDP Site 231 from the Gulf of Aden, has provided vegetation data going back 11.3 My (7).

Here, we present an ∼24-My vegetation record from carbon isotopes of *n*-alkane plant waxes from four marine cores that collectively span the Neogene to present. Volcanic ashes in the cores correlated to those deposited in the Turkana and Awash Basins provide evidence that plant waxes are sourced from eastern Africa (60). Vegetation data from the cores provide new insight into the timing, nature, and spatial patterns of C_4 grassland expansion in eastern Africa by significantly expanding the spatial and temporal range of existing data. Early and middle Miocene vegetation data from the Somali Basin address whether C_4 vegetation was present in Africa before the late Miocene. We use the carbon isotope data to evaluate the role of vegetation change in mammalian evolution, and we evaluate C_4 grassland expansion at the macroevolutionary scale in eastern Africa and in a global context.

Site Selection and Interpretive Framework

The four cores, from DSDP Sites 228, 232, 235, and 241, range in latitude from 19.1°N to 2.4°S (Fig. 1) and have basal ages of 3.9 Ma, 5.5 Ma, 13.5 Ma, and 23.4 Ma, respectively, from the sampled intervals. Age–depth models are shown in Fig. S1, data are given in Dataset S1, and methods are described in *SI Materials and Methods*. Sample ages, presented in Dataset S1, were interpolated using the age–depth models for each site based on calcareous nannofossil biostratigraphy updated to the most recent biohorizon ages (61, 62), and from radiometrically dated volcanic ashes in the cores (60). Each site was nominally sampled at ∼0.5- to 1.4-My resolution to capture long-term, Neogene paleovegetation trends and provide a broad temporal context to shorter but higher-resolution records from terrestrial and marine archives. DSDP site information for each core is given in Dataset S2 and sample lithologies are summarized in Dataset S3.

We interpret regional vegetation using carbon isotope data from the *n*-C_{31} alkane because it best reflects the actual distribution of

vegetation on the landscape. Garcin et al. (63) found that, among *n*-alkane homologs commonly measured for carbon isotopes, the concentration of the *n*-C_{31} alkane is nearly identical in C_3 and C_4 plants in Africa, effectively removing plant wax production biases related to plant functional type. However, the significant differences in concentrations of other *n*-alkane homologs between C_3 plants and C_4 grasses also contain powerful information for reconstructing vegetation. For example, C_4 grasses have higher concentrations of longer chain *n*-alkanes (C_{33} and C_{35}) than C_3 plants. Conversely, C_3 plants have higher concentrations shorter chain lengths (e.g., C_{27} or C_{29}) (63–65). Furthermore, C_{35} is absent in modern rainforest taxa, extremely low (~3% of total *n*-alkanes) in savanna trees, shrubs, and herbs, but relatively abundant (up to 20% of total *n*-alkanes) in C_4 grasses (64, 65). As a result, the $\delta^{13}C$ value of the *n*-C_{35} alkanes ($\delta^{13}C_{C35}$) is extremely responsive to the presence of C_4 vegetation on the landscape. This allows us to use the $\delta^{13}C$ value of the *n*-C_{35} alkane as a highly sensitive indicator of C_4 vegetation on the landscape. Additionally, the absence of the *n*-C_{35} alkane and dominance of the *n*-C_{29} alkane in plant wax molecular distributions are characteristic of modern rainforest plants (64). We suggest that similar patterns in *n*-alkane distributions from ancient sediments coupled with carbon isotope values representative of rainforest taxa would be indicative of rainforest vegetation in the past.

Results and Discussion

Concentration and carbon isotope data for the *n*-C_{29}, *n*-C_{31}, *n*-C_{33}, and *n*-C_{35} alkanes extracted from marine core sediments ($n = 46$) are presented in Datasets S4 and S5, respectively. Molecular distributions indicate long chain *n*-alkanes are derived from terrestrial plants (*SI Materials and Methods* and Fig. S2). The average chain length (ACL) and carbon preference index (CPI) are coarse metrics commonly used to evaluate plant wax distributions (Dataset S4). The former reflects the relative amounts of long and shorter *n*-alkanes, whereas the latter measures the strong biosynthetic preference for odd-numbered *n*-alkanes in plants versus the approximately equal preference in petroleum (see also *SI Materials and Methods*). The ACL and CPI for all samples are similar to modern African plant values (64), indicating *n*-alkanes are derived from terrestrial plants with no indications of significant diagenesis or addition of exogenous long chain *n*-alkanes (e.g., microbial sources or petrogenesis). The oldest sample analyzed, from Site 241, is characterized by a large unresolved complex mixture (UCM) in the range of short-chain to midchain lengths that does not appear to affect the $\delta^{13}C$ values of long-chain plant-derived *n*-alkanes (Fig. S2). Other samples exhibit small UCMs in the short-chain and midchain length range (Fig. S2).

We adopt the C_3 and C_4 carbon isotope endmember values for *n*-alkanes in African ecosystems compiled by Garcin et al. (63). For *n*-C_{31} alkanes, they are $-33.8 \pm 3.9‰$ (1σ) and $-20.1 \pm 2.5‰$, respectively, corrected to preindustrial atmospheric pCO_2 ($\delta^{13}C_{atm}$) values. Similarly, all $\delta^{13}C$ values presented here have been corrected to a preindustrial atmospheric pCO_2 value of –6.5 ‰ using estimated $\delta^{13}C_{atm}$ values from the past (58, 66) (Dataset S6). The range of $\delta^{13}C$ values in the *n*-C_{31} alkane ($\delta^{13}C_{C31}$) from the DSDP cores is from –33.9‰ to –24.3‰, spanning nearly the entire range of C_3 to C_4 ecosystems (Fig. 2). The *n*-C_{35} alkane displays an even wider range of $\delta^{13}C_{C35}$ values, from –33.3‰ to –22.0‰. (Dataset S5 and Fig. S3).

Carbon Isotope Values and Molecular Distributions from 24 Ma to 10 Ma. The $\delta^{13}C_{C31}$ values from 24 Ma to 10 Ma come from the Site 235 and 241 cores in the Somali Basin and are very depleted and nearly invariant, ranging from –33.9‰ to –32.2‰ (Fig. 2), indicative of C_3 ecosystems. The range of $\delta^{13}C_{C35}$ values before 10 Ma is similarly small, from –33.3‰ to –31.3‰ (Fig. S4 and Dataset S5). The other *n*-alkane homologs, C_{29} and C_{33}, have a pooled range of –34.0‰ to –30.8‰. Given the similarity in $\delta^{13}C$ values of the four homologs through time and the relative geographic proximity of Sites 235 and 241, we combine data from both sites into a single Somali Basin record (Fig. S4). Combining the two sites into a single record is further supported by clay mineralogy of the Somali Basin sediments, which indicates a similar sediment provenance of the Horn of Africa and possibly Central Africa for both sites (67). All values from Somali Basin samples are indicative of C_3 ecosystems in eastern Africa before 10 Ma. The limited range within each homolog from 20 Ma to 10 Ma suggests that the $\delta^{13}C$ values likely define endmember values for C_3 ecosystems in eastern Africa. The persistently low $\delta^{13}C$ values of the *n*-C_{35} homolog are particularly diagnostic, indicating no isotopic evidence for C_4 vegetation in east Africa from 24 Ma to 10 Ma.

The average molecular distribution of *n*-alkanes for pre-10-Ma samples has a *n*-C_{31} maximum, followed in order of abundance by *n*-C_{29}, *n*-C_{33}, *n*-C_{27}, and *n*-C_{35} (Fig. S5). Although the data do not preclude minor amounts of rainforest vegetation, the *n*-alkane distribution does not support widespread rainforests in eastern Africa, nor do measured $\delta^{13}C_{C31}$ values, which do not reach the low values characteristic of rainforest vegetation (see figure 6a in ref. 64 for reference *n*-alkane distributions). Rather, the molecular distributions and $\delta^{13}C_{C31}$ values reflect a combination of nonrainforest trees, shrubs, herbs, and C_3 grasses. Relative contributions of these C_3 plant types cannot be ascertained from the molecular distribution data. Two possible exceptions to this are the molecular distributions from samples from 19.18 Ma (Site 241, sample KU357) and 1.15 Ma (Site 228, sample KU315), which have distributions similar to modern rainforest plants (Fig. S6). However, the $\delta^{13}C$ values are –32.4‰ and –25.2‰, respectively, neither of which reflect modern rainforest plants values of $-35.6 \pm 2.8‰$ (corrected to preindustrial atmospheric $\delta^{13}C$ values) (64).

Comparing Biomarker Data with Existing Vegetation Records. The absence of C_4 vegetation at the regional scale before 10 Ma based on *n*-alkane carbon isotope and molecular distribution data is supported by vegetation reconstructions from paleobotanical

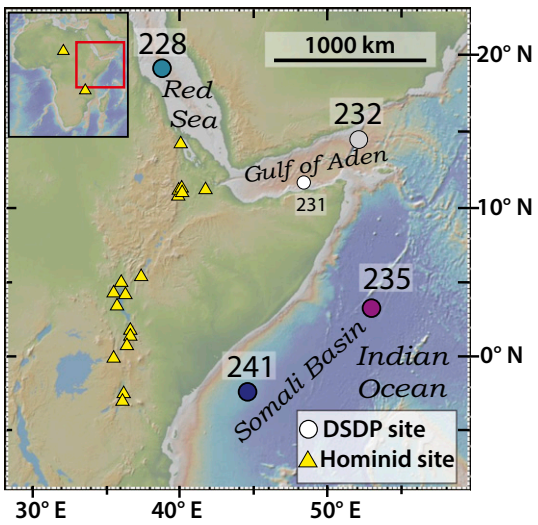

Fig. 1. Map of eastern Africa showing DSDP core Sites 228, 232, 235, and 241 sampled for this study. Previously studied Site 231 is also shown. Yellow triangles indicate hominid fossil localities from 10 Ma to 1 Ma. (*Inset*) The two hominin sites are Toros-Menalla (Chad, central Africa) and the Chiwondo Beds in the Karonga Basin of northern Malawi. Both sites may fall within the plant wax source regions for cores used in this study. Base map is from GeoMapApp (112, www.geomapapp.org).

records of predominantly forest or wooded ecosystems in Ethiopia, Kenya, and Uganda (15–17, 19, 27).

Notable exceptions from two sites in Kenya suggest minor amounts of C_4 grasses may have been present locally before 10 Ma (52, 68, 69). At these sites, isotopic evidence comes from pedogenic carbonate $\delta^{13}C$ ($\delta^{13}C_{PC}$) values, where C_3-dominated ecosystems have $\delta^{13}C_{PC}$ values ranging from −15‰ to −8‰, mixed C_3–C_4 ecosystems range from −8‰ to −2‰, and C_4-dominated ecosystems range from −2‰ to +4‰, after correction to preindustrial atmospheric $\delta^{13}C$ values.

A single pedogenic carbonate value from the Hiwegi Formation (17.8 Ma) on Rusinga Island in Lake Victoria has a $\delta^{13}C_{PC}$ value of −5.7‰ (68). However, the corresponding $\delta^{13}C$ value from coexisting soil organic matter is −24.3‰, consistent with water-stressed C_3 vegetation or minor amounts (*ca.* 15%) of C_4 vegetation. There is an enrichment in ^{13}C between soil organic matter and pedogenic carbonate that is a function of kinetic processes (diffusion of CO_2 in soils) and equilibrium isotopic exchange during carbonate precipitation that results in a theoretical enrichment of +14‰ to +17‰ (35). The observed enrichment factor of +18.6‰ for the Hiwegi Formation sample falls slightly outside this theoretical value. The other $\delta^{13}C_{PC}$ values that suggest C_4 vegetation existed before 10 Ma come from the Tugen Hills (Baringo Basin) in the central Kenyan Rift Valley (52, 69). Five pedogenic carbonates from the ∼15.5-Ma sediments in the Muruyur Formation have $\delta^{13}C_{PC}$ values ranging from −7.4‰ to −5.2‰. Only one of the five samples (MU 453, $\delta^{13}C_{PC}$ = −7.4‰) has a corresponding organic matter value with an enrichment value within the theoretical range of +14–17‰, making it the most reliable value from this period (70). Two $\delta^{13}C_{PC}$ values around −6.5‰ from the ∼10.5-Ma section of the Ngorora Formation, also in the Tugen Hills, indicate minor amounts of C_4 vegetation. A corresponding organic matter $\delta^{13}C$ value from one of the samples is −24.3‰, which falls within the range of water-stressed C_3 vegetation. Even if all pre-10-Ma pedogenic carbonate values >−8‰ are accepted and considered with other paleovegetation data from Rusinga and the Tugen Hills, the picture that emerges from both sites can be summarized as wooded to forested environments with minor amounts of C_4 vegetation present. The early presence of minor amounts of C_4 vegetation in eastern African is entirely consistent with an emergence of the C_4 photosynthetic pathway in the late Eocene or early Oligocene (71, 72). Despite an early emergence, C_4 grasses remained minor constituents of global ecosystems until their late Miocene expansion (73).

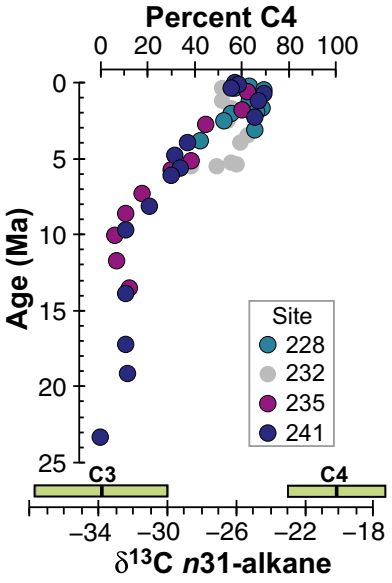

Fig. 2. Carbon isotope values of *n*-C_{31} alkanes indicate C_3 vegetation from 24 Ma to 10 Ma. After 10 Ma, the increase in $\delta^{13}C$ values reflects the increasing proportion of C_4 vegetation on the landscape. The near-linear increase in samples from the Somali Basin (DSDP Sites 235 and 241) and Red Sea (Site 228), suggest a regionally coherent expansion of C_4 vegetation. Percent C_4 is calculated from endmembers compiled in ref. 63. Large variability in endmember values leads to uncertainties in percent C_4 of 15–21% (Dataset S5). Uncertainty of measured $\delta^{13}C$ values, however, is much smaller (∼ ±0.10‰).

Fort Ternan (14 Ma) is the final middle Miocene site that warrants discussion, because well-preserved grass macrofossils were found there (18) and 54% of total pollen comes from grasses (27). Pedogenic carbonate values range from −14.9‰ to −9.8‰, leading to the conclusion that C_3 grasses were present at the site (74). Fort Ternan illustrates that, without plant fossils, whether from pollen, phytoliths, or macrofossils, C_3 grasses are invisible when viewed solely through an isotopic lens. The well-documented lack of pollen and the rarity of plant macrofossils in the Neogene of eastern Africa demonstrate the need to find other proxies that will enable us to investigate the Cenozoic history of grasses. Phytoliths could play a pivotal role; they have proven to be robust indicators of grasslands in the Cenozoic in other parts of the world (75). Other proxies for detecting C_3 grasses, where stable isotope methods are silent on the matter, include grass cuticles (76) or, possibly, *n*-alkane distributions (64, 65).

Onset of C_4 Grassland Expansion at 10 Ma and Effects on Fauna. The onset of C_4 grassland expansion in eastern Africa occurs at ∼10 Ma. It is marked by a sharp 3.1‰ increase in the $\delta^{13}C$ value of the *n*-C_{35} alkane that occurs between samples dated at 10.08 Ma and 9.65 Ma (Fig. 3). This is the first occurrence, to our knowledge, of a $\delta^{13}C$ value greater than −30‰ in the *n*-alkane record. Enrichment in ^{13}C occurs across all other alkane homologs with deceasing magnitude from C_{33} to C_{29} (Fig. S4), which follows the predicted pattern based on chemotaxonomic differences in *n*-alkane production observed in modern C_3 and C_4 plants in Africa (63) and unequivocally dates the onset of expansion of C_4 grasses in eastern Africa.

A remarkable consequence of the appearance of C_4 grass in eastern Africa is the immediate and, in some cases, dramatic dietary response of large herbivores (36). The *n*-alkane $\delta^{13}C$ values reveal a synchroneity between the onset of expansion of C_4 grasses and dietary shifts in proboscideans (Fig. 3) and other large herbivore lineages (36). Most striking is the shift from C_3-dominated to C_4-grazing diets in equids documented in Kenya between 9.9 Ma and 9.3 Ma. Other large mammals that followed suit by 9 Ma include bovids and rhinocerotids. Equids only arrived in Africa around 10.5 Ma, so there is no dietary record in eastern Africa for them in the earlier Neogene (59). Proboscideans, which include modern elephants and their ancestors, are an Afrotherian order for which dietary records exist from the early Miocene to present. Fig. 3 illustrates the dietary evolution of proboscideans from eastern and central (i.e., Chad) Africa over the past 17 My based upon carbon isotope data from their teeth (Dataset S7, compiled primarily from ref. 77). Small amounts of C_4 vegetation are present in proboscidean diets beginning at 9.9 Ma. The dominant early and middle Miocene proboscideans, Deinotheriidae and Gomphotheriidae, had brachydont molars with transverse lophs for shearing vegetation (78, 79). Although the inclusion of some C_3 grass in their diets cannot be ruled out, their craniodental morphology indicates they were browsers. If C_3 grasses were abundant at this time, proboscideans did not capitalize on this dietary resource and instead waited until the appearance of C_4 grasses at ∼10 Ma to begin grazing. In fact, as one of the dominant early Neogene herbivores, it is possible that browsing proboscideans maintained or even

increased grasslands, as their extant browsing relatives, *Loxodonta africana*, do today (80).

Carbon Isotope Data from 10 Ma to Present. **The nature of grassland expansion after 10 Ma.** The regional signal from the Somali Basin cores shows that C_4 vegetation increases linearly from 10 Ma to present (Fig. 2 and Fig. S7). Post-10-Ma $\delta^{13}C_{C31}$ values from the Somali Basin Sites 235 and 241 have nearly identical slopes, with R^2 values of 0.87 and 0.97, respectively (Fig. S7*A*). When combined, the Somali Basin samples yield a slope that indicates a $\delta^{13}C$ increase of 1.1‰ per million years (R^2_{C31} = 0.92) or 8.0% C_4 vegetation per million years (Fig. S7*B*). Adding the 10 samples from Site 228 (0.2–3.9 Ma) yields a similar trend, with an increase of +1.0‰ per million years (R^2_{C31} = 0.88) or 7.3% C_4 vegetation per million years. From 9.7 Ma to 5.1 Ma, Somali Basin $\delta^{13}C_{C31}$ values increase by 3.8‰, whereas $\delta^{13}C_{C33}$ and $\delta^{13}C_{C35}$ increase by 5.3‰ and 5.0‰, respectively, indicating significant increases in C_4 biomass during the late Miocene.

Molecular distributions suggest the increase in C_4 biomass detected from plant wax isotopes reflects increases in grasses rather than C_4 shrubs, such as arid-adapted shrubs found in the families Chenopodiaceae and Amaranthaceae. This is because the marked increase in *n*-C_{33} and *n*-C_{35} alkane relative abundances in post-10-Ma samples (Fig. S5) resembles *n*-alkane distributions in extant African C_4 grasses (65), whereas limited data of *n*-alkane distributions from C_4 shrubs (*Amaranthaceae* spp.) show they produce little to no *n*-C_{33} and *n*-C_{35} alkanes (81). We therefore interpret the increase in $\delta^{13}C$ values and relative abundances of *n*-C_{33} and *n*-C_{35} alkanes after 10 Ma to primarily reflect an increase in C_4 grasses. Interestingly, pollen from Chenopodiaceae and Amaranthaceae occurs in variable and occasionally high proportions (20–80%) in the late Miocene to Pliocene pollen record from DSDP 231 (9). Crassulacean acid metabolism (CAM) plants can have $\delta^{13}C$ values more positive than C_3 plants; however, today, their overall contribution to biomass in the region is small. Thus, CAM plants likely contributed minor or insignificant amounts of *n*-alkanes to the sediments in the Somali Basin cores (Sites 235 and 241).

Carbon isotope data from Sites 228 and 232 encompass the latter part of the C_4 expansion period and lie geographically much farther north than Sites 235 and 241 (Fig. 1). Unlike the deep water Somali Basin sites, sediments from Site 228 in the Red Sea include fluvial sediments from the (paleo) Sudanese Delta (82). Site 228 samples have a higher CPI (generally >8) than samples from the other three sites (Dataset S4), probably related to differences in plant wax source and fluvial transport and depositional processes. Despite the vast distance separating the Somali Basin from the Red Sea, carbon isotope values from the two regions follow the same trend (Fig. 2).

Site 232 is located at the eastern entrance to the Gulf of Aden close to the Arabian Peninsula (Fig. 1). The $\delta^{13}C_{C31}$ values from this site, with an estimated age of 5.54–0.39 Ma, range from −28.5‰ to −25.3‰. Although the core contains at least four ash layers correlated to the Turkana Basin (60), it is also highly likely that there is plant wax input from the Arabian Peninsula and, to a lesser extent, Southern Asia. This is based on the proximity to those areas and regional wind patterns (e.g., figure 1 in ref. 83). Provenance studies from nearby marine cores support this interpretation (84, 85). The Arabian Peninsula and Southern Asia (i.e., the Siwaliks) both had significant amounts of C_4 vegetation by 6 Ma, and therefore it is impossible to disentangle contributions from the three source areas (51, 86). Because of this potential complication, we refrain from making any interpretation of eastern Africa vegetation based on data from Site 232.

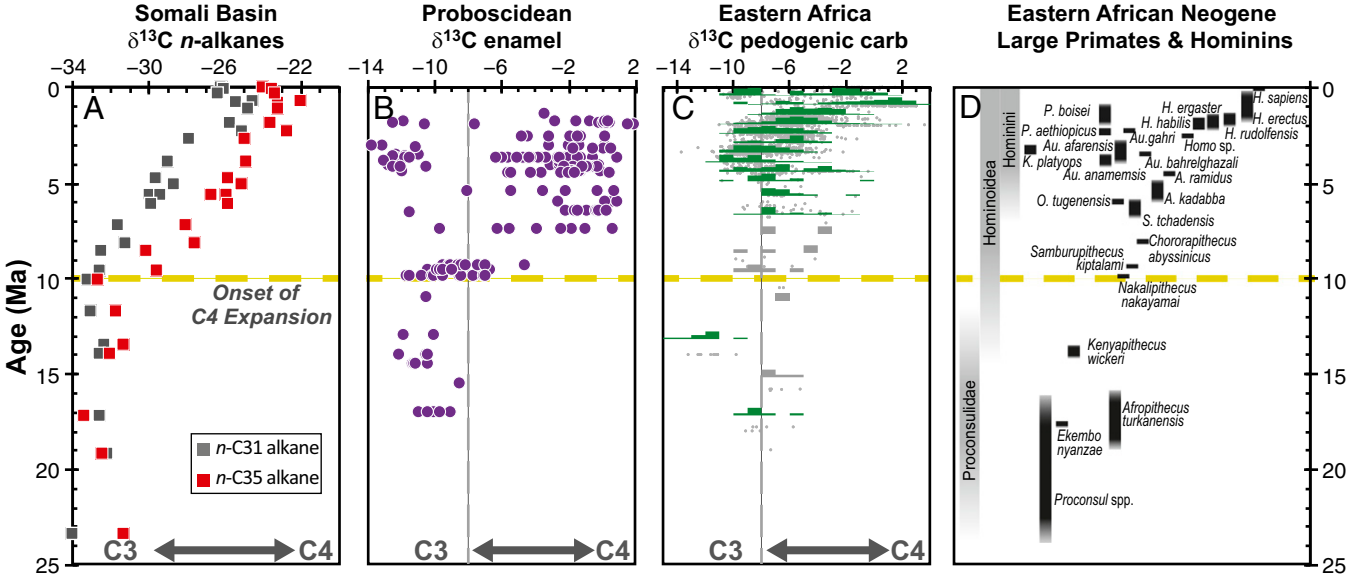

Fig. 3. Multiproxy carbon isotope data from eastern Africa illustrate the onset of the expansion of C_4 vegetation at 10 Ma and the dietary response of proboscideans. (*A*) Carbon isotope data from Somali Basin cores show a 3.1‰ increase in the *n*-C_{35} alkane at 10 Ma marking the onset of expansion of C_4 vegetation. Carbon isotope values from *n*C_{31}- and *n*C_{35}-alkanes increase from 10 Ma to present. (*B*) Tooth enamel $\delta^{13}C$ data from east and central African proboscideans (from many of the same locations as hominids in Fig 1) have C_3-dominated diets (<−8‰) from 17 Ma to 10 Ma, after which there is an immediate increase in $\delta^{13}C$ at 9.9 Ma from the inclusion of minor amounts of C_4 vegetation into their diet. Data are compiled from refs. 77 and 36. Other mammalian lineages that had C_4 vegetation in their diets by ∼9.6 Ma include equids, bovids, and rhinocerotids. (*C*) Pedogenic carbonate $\delta^{13}C$ data from eastern African fossil localities (see ref. 88 for sites) represent local vegetation conditions. Gray circles are individual data points; histograms draw from 2-My bins from 19 Ma to 10 Ma, 1-My bins from 10 Ma to 6 Ma, and 0.5-My bins from 6 Ma to 1 Ma. Bins with less than five data points are shown in gray. Data are compiled from refs. 88 and 89. Vertical dashed gray lines at −8‰ in *B* and *C* indicate the boundary between C_3 and mixed C_3–C_4 values. (*D*) Schematic of selected Neogene large-bodied primate taxonomy from eastern Africa. Probable and confirmed taxa of the subtribe homonini (7 Ma to present) occur after the onset of C_4 grassland expansion at 10 Ma. Taxa and age ranges are compiled from refs. 11, 91, and 113–116.

Comparison with existing paleoenvironmental data from 10 Ma to present. An extensive carbon isotope record from plant wax biomarkers exists for another Gulf of Aden core, Site 231, which is situated closer to the Horn of Africa than Site 232 (7). Site 231 biomarker data come from *n*-C_{30} alkanoic acids, also derived from terrestrial plants, but with different isotope systematics and end-member values than *n*-C_{31} alkanes (87). Despite these differences, general comparisons can be drawn between the two biomarker data sets. Both show an overall trend toward more positive $\delta^{13}C$ values through time from ∼10 Ma to present (Fig. S4). The Somali Basin data exhibit a larger range (9.5‰ in the *n*-C_{31} alkane, from −33.9‰ to −24.4‰) than Site 231 data (7.9‰ in the *n*-C_{30} acid, from −30.2‰ to −22.3‰), despite the former having a smaller sample size ($n = 26$) than the latter ($n = 372$). The absence of 24- to 12-Ma data from Site 231, a period characterized by exclusively C_3 vegetation, may explain the lack of more negative values characteristic of the *n*-alkane data in the early Neogene (Fig. S4 and Dataset S5). Site 231 $\delta^{13}C$ values are generally more positive than the $\delta^{13}C_{C31}$ values, probably, in part, due to differences in the lipid types (*n*-C_{31} alkane vs. *n*-C_{30} alkanoic acids). It may also be a result of different plant wax source areas. Site 231 $\delta^{13}C$ values exhibit high variability over short timescales (∼10–40 ky) associated with orbitally driven vegetation change in eastern Africa.

One curious feature of our records is a notable lack of variability that might be anticipated to result from undersampling (aliasing) of orbital-scale climate variability. Where sampling resolution was adequate to resolve such higher-frequency changes, plant wax biomarker records from Gulf of Aden Site 231 document large (±2–3‰) orbital-scale cycles over the last 4.5 Ma. Orbitally driven vegetation change has also been documented in lacustrine sediments from Olduvai Gorge (8). However, our low-resolution (∼0.5- to 1.4-My sampling) records consistently document gradual, smooth increases in C_4 vegetation from 10 Ma to present (Fig. 2). Given that large, orbital-scale variability is observed in marine and terrestrial archives when sedimentation rates are high and sequences are adequately sampled (7, 8, 44), we conclude that some other factor may be smoothing or obscuring this orbital signal in our records. All of our sites were rotary drilled and, in some cases, spot cored, and coring-related disturbance was observed in places. The Somali Basin average sedimentation rates are low (2–3 cm/ky), so bioturbation may have blurred orbital-scale variability. These sites are also quite distal from the coast, and so the plant wax catchment areas are likely quite large, implicating large spatial averaging as well. What is remarkable, however, is the uniformity of the C_4 expansion timing and the slopes of the C_4 expansion trends observed across all sites (Fig. S7).

There are numerous isotopic records from pedogenic carbonate from the Plio-Pleistocene of eastern Africa and several from the late Miocene available for comparison with the Somali Basin *n*-alkane data. We use the $\delta^{13}C_{PC}$ data set from eastern Africa recently compiled by Levin (88) and include new data added from the Karonga Basin in northern Malawi, a fossil locality that critically links eastern and southern African hominin sites (89) (Fig. 3*C*). We include the Malawi data because of its proximity to Site 241 and therefore likelihood of being part of the plant wax source area.

Data from the Tugen Hills (9.4–5 Ma) range from −9.3‰ to −4.2‰ and have a mean of −7.5 ± 1.3‰ (1σ). These values indicate C_3-dominated to mixed C_3–C_4 ecosystems (52, 55). At Lothagam, a site located in the Turkana Basin, $\delta^{13}C_{PC}$ values come from a slightly narrower age window of 8.4–5.7 Ma. They range from −9.0‰ to −1.3‰ with a mean of −5.0 ± 2.1‰ (90). At Lothagam, the landscape was more open than the Tugen Hills, with values reflecting mostly mixed C_3–C_4 to C_4-dominated ecosystems. Major increases in the number of species and the abundance of grazing mammals in the Turkana, Baringo, and Awash Basins during this period provide supporting evidence for the increase C_4 biomass and it's increasing significance as a dietary resource for African mammals (36, 41, 43).

Pedogenic carbonate records from 5 Ma to 1 Ma are abundant from hominin sites in eastern Africa, particularly from the Turkana and Awash Basins (4). The main trend is a shift toward increased C_4 vegetation from ∼4 Ma onward (Fig. 3*C*). Initially, the range of environments mainly comprises C_3-dominated to mixed C_3–C_4 ecosystems until about ∼2 Ma, when C_4-dominated ecosystems become more prevalent and C_3-dominated ecosystems essentially disappear from the record, with the exception of the Karonga Basin in northern Malawi (Fig. 3*C*). The diets of large herbivores in the Turkana Basin reflect this transition. From 4.1 Ma to 2.35 Ma, the fossil record is made up of taxa primarily with mixed C_3–C_4 diets and transitions to one comprised of mostly C_4 grazers from 2.35 Ma to 1 Ma (37). Both diet and vegetation reconstructions from terrestrial sites are in agreement with the Somali Basin *n*-alkane data, which indicate continued increases in C_4 vegetation through the Plio-Pleistocene.

Vegetation Change and Human Evolution. The earliest purported hominins, *Sahelanthropus tchadensis* and *Orrorin tugenensis*, appeared in the late Miocene (7–6 Ma) (Fig. 3*D*). By that time (6.5 Ma), the Somali Basin *n*-alkane data show an increase to 19% C_4 vegetation on the landscape, or a 2.6‰ increase in $\delta^{13}C_{C31}$ values above average early Neogene C_3 values based on the linear regression equation for all data (Fig. S7*C*). An even greater increase of 4.6‰ occurs in $\delta^{13}C_{C35}$ values by this time. These two early possible hominins emerged amid a period of major change in faunal communities and diets driven by changes in ecosystem structure associated with the expansion of C_4 grasses. The dietary shift toward C_4 grazing was well underway in many mammalian lineages (36, 43), but there are not yet any isotopic analyses of teeth to ascertain the diets of these early hominids.

However, extensive isotopic data from Plio-Pleistocene hominin teeth provide a clear picture of diets in different lineages, temporal trends, and dietary niche partitioning between Pleistocene genera (91–96). Two early species (4.4–4 Ma), *Ardipithecus ramidus* and *Australopithecus anamensis*, are anomalous for their C_3-dominated diets (−11.6‰ to −8.5‰). After 3.8 Ma, *Australopithecines* and *Kenyanthropus platyops* show a dramatic increase in isotopic range and, presumably, dietary breadth, with $\delta^{13}C$ values ranging from −13‰ to −2.7‰. *Australopithecus bahrelghazali* from Toros-Menalla (Chad, central Africa) shows the earliest evidence, to date (3.6 Ma), of a hominin with a consistent, mostly C_4-based diet (range −4.4‰ to −0.8‰). It is possible that the dietary evolution of central African hominins differed from those in eastern Africa, as is the case with the southern African hominins (97). In eastern Africa, the diet of *Paranthropus* evolves to become dependent on C_4-based foods from 2.7 Ma to 1.5 Ma (92). Overall, the increase in C_4-based foods in eastern African hominin diets mirrors the increasing prevalence of C_4 biomass on the landscape. Our genus, *Homo*, does not follow this trend.

The isotopic range of *Homo* diet remains variable and broad (−9.9‰ to −2.2‰, mean = 6.1‰), indicating dietary flexibility from ∼2.4 Ma to 1.3 Ma (95). Microwear studies suggest dietary differences between *Homo* species based on tooth wear, supporting the broad isotopic range (98). An important observation, then, is that *Homo* diet remained flexible during a time of rising environmental inflexibility imposed by increasing aridity and C_4 vegetation on the landscape. One critical element of hominin diet that remains unknown, and is especially important for *Homo,* is when meat became an important food source. Carbon isotopes do not provide information on trophic level; thus isotope-based reconstructions of hominin diet reflect some combination of plant foods and of higher trophic level foods such as insects, mammals, or aquatic fauna.

The plant wax data from the Somali Basin, along with pedogenic carbonate and Gulf of Aden (Site 231) plant wax data, show that

continued increases in the proportion of C_4 grasses on the landscape ultimately influenced hominin diet, possibly from the inception of the lineage. The shift to more open environments presented hominins with new challenges as to how they acquired their food, avoided predators, and managed higher heat loads. The challenges posed by the changing environmental conditions were met with changes to diet (C_4-based foods and, eventually, meat), the innovation of tools, and, ultimately, increased social complexity such as the cooperative acquisition of resources through foraging, scavenging, or hunting.

Global Context of C_4 Grassland Expansion in Eastern Africa. The Neogene plant wax record provides the opportunity to place the expansion of C_4 grasslands in eastern Africa into a global context. C_4 grassland expansion has been investigated most intensively in the Siwaliks of South Asia (48, 51, 53), the Americas (49, 54, 99–101), southern Africa (102, 103), and, to a lesser degree, China (104, 105), the Mediterranean (106), and the Middle East (85, 86). The onset of expansion at 10 Ma in eastern Africa precedes by at least 2 My that of well-dated terrestrial records from the Siwaliks (~8 Ma), North and South America (~8–6 Ma), and South Africa (~8–7 Ma).

An important feature of the eastern Africa biomarker record is that it captures the transition from isotopically invariant C_3-dominated ecosystems during the first part of the Neogene to the period of dynamic change after 10 Ma (Fig. 2). The expansion of C_4 grasslands in eastern Africa differs markedly from other regions around the world in its earlier onset and the monotonic increase in C_4 grasses at the regional scale. The mode of expansion differs from the step-like change that occurred in the Siwaliks, arguably the most well documented case of grassland expansion (51). It also differs from the Great Plains of North America, which shows possible minor amounts of C_4 vegetation as early as ~23 Ma but an expansion beginning around 7 Ma, based on the pedogenic carbonate record (54). A North American vegetation reconstruction from *n*-C_{31} alkane data from a Gulf of Mexico core (DSDP Site 94) also suggests minor amounts of C4 vegetation by 9.1 Ma or possibly earlier (49). Two marine sediments cores (Ocean Drilling Program Sites 1081 and 1085) spanning ~10 degrees of latitude from southern Africa both indicate the onset of expansion at ~7.5 Ma based on *n*-C_{31} alkane data, lagging eastern Africa by ~2.5 My (102, 103). A Neogene vegetation record from western Africa could provide information on mechanisms behind the expansion in Africa because it would show whether or not expansion occurred synchronously across eastern and western Africa. Clearly, there is the need for continued efforts to produce well-dated records of C_4 expansion to identify additional regional, continental, or global patterns. This includes characterizing the vegetation and climatic conditions before the expansion, which were not uniform globally. Improved spatial and chronological resolution will greatly enhance our understanding of the driving mechanisms of grassland expansion.

Commonly invoked causes for C_4 grassland expansion include a late Miocene decrease in atmospheric CO_2 concentrations (pCO_2) or increases in aridity, seasonality of precipitation, fire, and herbivory (56, 107–109). These factors are not mutually exclusive; therefore, debate continues about the relative importance of each variable (110). Most are difficult to quantify in the geologic record, and all continue to benefit from new or improved proxy methods for reconstruction in deep time. This includes characterizing fire frequency and intensity, identifying C_3 grass abundance, quantifying seasonality and aridity, and refining pCO_2 estimates.

Conclusions

The Neogene *n*-alkane carbon isotope record from the Somali Basin shows no evidence for C_4 vegetation at the regional scale during the early or middle Miocene of eastern Africa, which is consistent with terrestrial isotopic, faunal, and floral records. The first evidence of C_4 vegetation is indicated by a 3.1‰ increase in the *n*-C_{35} alkane homolog at 10 Ma. Molecular distributions suggest the increase in C_4 biomass was from grasses rather than from arid-adapted C_4 shrubs. From 10 Ma to present, C_4 grasses increase monotonically on the landscape at the regional scale, as evidenced in the agreement between $\delta^{13}C$ records in cores stretching from the Somali Basin to the Red Sea. Despite the strong secular trend in the *n*-alkane marine core records, terrestrial records document persistent vegetation heterogeneity at the local scale, and the Site 231 biomarker record demonstrates dramatic vegetation changes driven by orbital cyclicity. Collectively, the *n*-alkane vegetation record and dietary reconstructions show that vegetation change beginning at 10 Ma influenced the evolution of mammalian diets and, later, hominin diets. The Somali Basin record demonstrates that C_4 grassland expansion in eastern Africa was different in timing and mode from other regions in the world. Although this does not preclude common, global phenomena (e.g., pCO_2) as important drivers or preconditions to the global expansion of C_4 grasslands, it further underscores regional variables as critical determinants for the timing and mode of late Neogene vegetation change.

Materials and Methods

All isotopic data are presented in delta notation, where $\delta^{13}C = ([^{13}C/^{12}C_{sample}]/[^{13}C/^{12}C_{standard}] - 1)$ and the standard is VPDB. Plant waxes were extracted from cleaned and crushed marine sediments with organic solvents. The *n*-alkanes were isolated by silica gel column chromatography, identified by gas chromatography mass spectrometry, and quantified by comparison with an internal standard and standard mixtures of C_8–C_{40} *n*-alkanes. Carbon isotope ratios were measured using a gas chromatography–combustion interface coupled to an isotope ratio mass spectrometer. Carbon isotopes values were corrected based on values of isotopic standards using the methods of Polissar and D'Andrea (111). *SI Materials and Methods* contains a more detailed description of organic geochemical and stable isotope methods.

Acknowledgments

We acknowledge shipboard parties responsible for recovering and describing cores from the DSDP Sites 228, 232, 235, and 241, because nearly all sites lie within what, today, are pirate-infested waters that preclude recovery of new cores. We thank two anonymous reviewers for constructive comments, the International Ocean Discovery Program's Kochi Core Center for providing samples for this study, and Mark Franklin for laboratory assistance. Funding was provided by the Center for Climate and Life at the Lamont-Doherty Earth Observatory (LDEO) of Columbia University. K.E.J.'s participation through the LDEO summer undergraduate internship program was supported by US National Science Foundation Grant OCE-1359194. This is Lamont-Doherty Earth Observatory Contribution 8001.

1 Glazko GV, Nei M (2003) Estimation of divergence times for major lineages of primate species. *Mol Biol Evol* 20(3):424–434.
2 Chen F-C, Li W-H (2001) Genomic divergences between humans and other hominoids and the effective population size of the common ancestor of humans and chimpanzees. *Am J Hum Genet* 68(2):444–456.
3 Levin NE, Brown FH, Behrensmeyer AK, Bobe R, Cerling TE (2011) Paleosol carbonates from the Omo Group: Isotopic records of local and regional environmental change in East Africa. *Palaeogeogr Palaeoclimatol Palaeoecol* 307(1-4):75–89.
4 Cerling TE, et al. (2011) Woody cover and hominin environments in the past 6 million years. *Nature* 476(7358):51–56.
5 WoldeGabriel G, et al. (2009) The geological, isotopic, botanical, invertebrate, and lower vertebrate surroundings of *Ardipithecus ramidus*. *Science* 326(5949):65–65e5.
6 Bamford MK (2011) Fossil leaves, fruits and seeds. *Paleontology and Geology of Laetoli: Human Evolution in Context*, ed Harrison T (Springer, New York), pp 235–252.
7 Feakins SJ, et al. (2013) Northeast African vegetation change over 12 My. *Geology* 41(3):295–298.
8 Magill CR, Ashley GM, Freeman KH (2013) Ecosystem variability and early human habitats in eastern Africa. *Proc Natl Acad Sci USA* 110(4):1167–1174.
9 Bonnefille R (2010) Cenozoic vegetation, climate changes and hominid evolution in tropical Africa. *Global Planet Change* 72(4):390–411.

10 Jacobs BF, Pan AD, Scotese CR (2010) A review of the Cenozoic vegetation history of Africa. *Cenozoic Mammals of Africa*, eds Werdelin L, Sanders W (Univ Calif Press, Berkeley, CA), pp 57–72.
11 Levin NE (2015) Environment and climate of early human evolution. *Annu Rev Earth Planet Sci* 43(1):405–429.
12 Jacobs BF, Deino AL (1996) Test of climate-leaf physiognomy regression models, their application to two Miocene floras from Kenya, and 40Ar39Ar dating of the Late Miocene Kapturo site. *Palaeogeogr Palaeoclimatol Palaeoecol* 123(1):259–271.
13 Dechamps R, Senut B, Pickford M (1992) Fruits fossiles pliocènes et pléistocènes du Rift occidental ougandais. Signification paléoenvironnementale. *C R Acad Sci Ser 2* 314(3):325–331.
14 Albert RM, Bamford MK, Cabanes D (2006) Taphonomy of phytoliths and macroplants in different soils from Olduvai Gorge (Tanzania) and the application to Plio-Pleistocene palaeoanthropological samples. *Quat Int* 148(1):78–94.
15 Jacobs BF, Kabuye CH (1987) A middle Miocene (12·2 My old) forest in the East African Rift Valley, Kenya. *J Hum Evol* 16(2):147–155.
16 Chesters KI (1957) *The Miocene Flora of Rusinga Island* (Palaeontographica, Lake Victoria, Kenya), pp 30–71.
17 Tiffney BH, Fleagle JG, Bown TM (1994) Early to Middle Miocene angiosperm fruits and seeds from Fejej, Ethiopia. *Tertiary Research* 15(1):25–42.
18 Retallack GJ, Dugas DP, Bestland EA (1990) Fossil soils and grasses of a middle Miocene East African grassland. *Science* 247(4948):1325–1328.
19 Collinson ME, Andrews P, Bamford MK (2009) Taphonomy of the early Miocene flora, Hiwegi Formation, Rusinga Island, Kenya. *J Hum Evol* 57(2):149–162.
20 Michel LA, et al. (2014) Remnants of an ancient forest provide ecological context for Early Miocene fossil apes. *Nat Commun* 5:3236.
21 Bonnefille R, Potts R, Chalié F, Jolly D, Peyron O (2004) High-resolution vegetation and climate change associated with Pliocene *Australopithecus afarensis*. *Proc Natl Acad Sci USA* 101(33):12125–12129.
22 Bonnefille R (1994) Palynology and paleoenvironment of East African hominid sites. *Integrative Paths to the Past: Paleoanthropological Advances in Honor of F. Clark Howell*, eds Corruccini RS, Ciochon RL (Pearson, Englewood Cliff, NJ), pp 415–427.
23 Bonnefille R (1995) A reassessment of the Plio-Pleistocene pollen record of East Africa. *Paleoclimate and Evolution, with Emphasis on Human Origins* (Yale Univ Press, New Haven, CT), pp 299–310.
24 Dupont LM, Agwu CO (1991) Environmental control of pollen grain distribution patterns in the Gulf of Guinea and offshore NW-Africa. *Geol Rundsch* 80(3):567–589.
25 Prentice IC (1985) Pollen representation, source area, and basin size: Toward a unified theory of pollen analysis. *Quat Res* 23(1):76–86.
26 Bonnefille R (1976) Implications of pollen assemblage from the Koobi Fora formation, East Rudolf, Kenya. *Nature* 264(5585):403–407.
27 Bonnefille R (1984) Cenozoic vegetation and environments of early hominids in East Africa. *The Evolution of the East Asian Environment*, ed White RO (Univ Hong Kong, Hong Kong), Vol 2, pp 579–612.
28 Twiss PC, Suess E, Smith RM (1969) Morphological classification of grass phytoliths. *Soil Sci Soc Am J* 33(1):109–115.
29 Rossouw L, Scott L (2011) Phytoliths and pollen, the microscopic plant remains in Pliocene volcanic sediments around Laetoli, Tanzania. *Paleontology and Geology of Laetoli: Human Evolution in Context*, ed Harrison T (Springer, New York), pp 201–215.
30 Barboni D, Bonnefille R, Alexandre A, Meunier J-D (1999) Phytoliths as paleoenvironmental indicators, west side Middle Awash Valley, Ethiopia. *Palaeogeogr Palaeoclimatol Palaeoecol* 152(1):87–100.
31 Bender M (1971) Variations in the $^{13}C/^{12}C$ ratios of plants in relation to the pathway of photosynthetic carbon dioxide fixation. *Phytochemistry* 10(6):1239–1244.
32 Tieszen LL, Senyimba MM, Imbamba SK, Troughton JH (1979) The distribution of C_3 and C_4 grasses and carbon isotope discrimination along an altitudinal and moisture gradient in Kenya. *Oecologia* 37(3):337–350.
33 Livingstone D, Clayton W (1980) An altitudinal cline in tropical African grass floras and its paleoecological significance. *Quat Res* 13(3):392–402.
34 Cerling TE (1984) The stable isotopic composition of modern soil carbonate and its relationship to climate. *Earth Planet Sci Lett* 71(2):229–240.
35 Cerling TE, Quade J (1993) Stable carbon and oxygen isotopes in soil carbonates. *Climate Change in Continental Isotopic Records*, Geophysical Monograph Series, eds Swart PK, Kohmann KC, Mckenzie J, Savin S (Am Geophys Union, Washington, DC), Vol 78, pp 217–231.
36 Uno KT, et al. (2011) Late Miocene to Pliocene carbon isotope record of differential diet change among East African herbivores. *Proc Natl Acad Sci USA* 108(16):6509–6514.
37 Cerling TE, et al. (2015) Dietary changes of large herbivores in the Turkana Basin, Kenya from 4 to 1 Ma. *Proc Natl Acad Sci USA* 112(37):11467–11472.
38 Lee-Thorp JA, van der Merwe NJ (1991) Aspects of the chemistry of modern and fossil biological apatites. *J Archaeol Sci* 18(3):343–354.
39 DeNiro MJ, Epstein S (1978) Influence of diet on the distribution of carbon isotopes in animals. *Geochim Cosmochim Acta* 42(5):495–506.
40 Cerling T, Harris J (1999) Carbon isotope fractionation between diet and bioapatite in ungulate mammals and implications for ecological and paleoecological studies. *Oecologia* 120(3):347–363.
41 Levin NE, Simpson SW, Quade J, Cerling TE, Frost SR (2008) Herbivore enamel carbon isotopic composition and the environmental context of Ardipithecus at Gona, Ethiopia. *Spec Pap Geol Soc Am* 446:215–234.
42 Zazzo A, et al. (2000) Herbivore paleodiet and paleoenvironmental changes in Chad during the Pliocene using stable isotope ratios of tooth enamel carbonate. *Paleobiology* 26(2):294–309.
43 Roche D, Ségalen L, Senut B, Pickford M (2013) Stable isotope analyses of tooth enamel carbonate of large herbivores from the Tugen Hills deposits: Palaeoenvironmental context of the earliest Kenyan hominids. *Earth Planet Sci Lett* 381:39–51.
44 Uno KT, et al. (2016) A Pleistocene paleovegetation record from plant-wax biomarkers from the Nachukui Formation, West Turkana, Kenya. *Philos Trans R Soc Lond B Biol Sci*, 10.1098/rstb.2015.0235.
45 Eglinton G, Hamilton RJ (1967) Leaf epicuticular waxes. *Science* 156(3780):1322–1335.
46 Cox R, Mazurek M, Simoneit B (1982) Lipids in Harmattan aerosols of Nigeria. *Nature* 296(5860):848–847.
47 Simoneit BR (1977) Biogenic lipids in particulates from the lower atmosphere over the eastern Atlantic. *Nature* 267(5613):682–685.
48 Freeman KH, Colarusso LA (2001) Molecular and isotopic records of C_4 grassland expansion in the late miocene. *Geochim Cosmochim Acta* 65(9):1439–1454.
49 Tipple BJ, Pagani M (2010) A 35 Myr North American leaf-wax compound-specific carbon and hydrogen isotope record: Implications for C_4 grasslands and hydrologic cycle dynamics. *Earth Planet Sci Lett* 299(1):250–262.
50 Edwards EJ, et al.; C_4 Grasses Consortium (2010) The origins of C_4 grasslands: Integrating evolutionary and ecosystem science. *Science* 328(5978):587–591.
51 Quade J, Cerling TE, Bowman JR (1989) Development of Asian monsoon revealed by marked ecological shift during the latest Miocene in northern Pakistan. *Nature* 342(6246):163–166.
52 Kingston JD, Hill A, Marino BD (1994) Isotopic evidence for neogene hominid paleoenvironments in the Kenya Rift Valley. *Science* 264(5161):955–959.
53 Quade J, Cater JM, Ojha TP, Adam J, Harrison TM (1995) Late Miocene environmental change in Nepal and the northern Indian subcontinent: Stable isotopic evidence from paleosols. *Geol Soc Am Bull* 107(12):1381–1397.
54 Fox DL, Koch PL (2003) Tertiary history of C_4 biomass in the Great Plains, USA. *Geology* 31(9):809–812.
55 Cerling TE (1992) Development of grasslands and savannas in East Africa during the Neogene. *Global Planet Change* 5(3):241–247.
56 Cerling TE, et al. (1997) Global vegetation change through the Miocene/Pliocene boundary. *Nature* 389(6647):153–158.
57 Morgan M, Kingston J (1994) Carbon isotopie evidence for the emergence of C_4 plants in the Neogene from Pakistan and Kenya. *Nature* 367:162–165.
58 Passey BH, et al. (2002) Environmental change in the Great Plains: An isotopic record from fossil horses. *J Geol* 110(2):123–140.
59 Bernor RL, Kaiser TM, Nelson SV (2004) The oldest Ethiopian Hipparion (Equinae, Perissodactyla) from Chorora; systematics, paleodiet and paleoclimate. *Cour Forschungsinst Senckenberg* 246:213–226.
60 Brown FH, Sarna-Wojcicki AM, Meyer CE, Haileab B (1992) Correlation of Pliocene and Pleistocene tephra layers between the Turkana Basin of East Africa and the Gulf of Aden. *Quat Int* 13/14(C):55–67.
61 Raffi I, et al. (2006) A review of calcareous nannofossil astrobiochronology encompassing the past 25 million years. *Quat Sci Rev* 25(23):3113–3137.
62 Backman J, Raffi I, Rio D, Fornaciari E, Pälike H (2012) Biozonation and biochronology of Miocene through Pleistocene calcareous nannofossils from low and middle latitudes. *Newsl Stratigr* 45(3):221–244.
63 Garcin Y, et al. (2014) Reconstructing C_3 and C_4 vegetation cover using *n*-alkane carbon isotope ratios in recent lake sediments from Cameroon, Western Central Africa. *Geochim Cosmochim Acta* 142:482–500.
64 Vogts A, Moossen H, Rommerskirchen F, Rullkötter J (2009) Distribution patterns and stable carbon isotopic composition of alkanes and alkan-1-ols from plant waxes of African rain forest and savanna C_3 species. *Org Geochem* 40(10):1037–1054.

65 Rommerskirchen F, Plader A, Eglinton G, Chikaraishi Y, Rullkötter J (2006) Chemotaxonomic significance of distribution and stable carbon isotopic composition of long-chain alkanes and alkan-1-ols in C_4 grass waxes. *Org Geochem* 37(10):1303–1332.
66 Tipple B, Meyers S, Pagani M (2010) Carbon isotope ratio of Cenozoic CO_2: A comparative evaluation of available geochemical proxies. *Paleoceanography* 25(3):PA3202.
67 Kolla V, Henderson L, Biscaye PE (1976) Clay mineralogy and sedimentation in the western Indian Ocean. *Deep Sea Res Oceanogr Abstr* 23(10):949–961.
68 Bestland EA, Krull ES (1999) Palaeoenvironments of Early Miocene Kisingiri volcano Proconsul sites: Evidence from carbon isotopes, palaeosols and hydromagmatic deposits. *J Geol Soc Lond* 156(5):965–976.
69 Behrensmeyer AK, Deino AL, Hill A, Kingston JD, Saunders JJ (2002) Geology and geochronology of the middle Miocene Kipsaramon site complex, Muruyur Beds, Tugen Hills, Kenya. *J Hum Evol* 42(1-2):11–38.
70 Kingston JD (1992) Stable isotopic evidence for hominid paleoenvironments in East Africa. Ph.D. dissertation (Harvard Univ, Cambridge, MA).
71 Urban MA, et al. (2010) Isotopic evidence of C4 grasses in southwestern Europe during the Early Oligocene–Middle Miocene. *Geology* 38(12):1091–1094.
72 Vicentini A, Barber JC, Aliscioni SS, Giussani LM, Kellogg EA (2008) The age of the grasses and clusters of origins of C_4 photosynthesis. *Global Change Biol* 14(12):2963–2977.
73 Sage RF (2004) The evolution of C_4 photosynthesis. *New Phytol* 161(2):341–370.
74 Cerling TE, Quade J, Ambrose SH, Sikes NE (1991) Fossil soils, grasses, and carbon isotopes from Fort Ternan, Kenya: Grassland or woodland? *J Hum Evol* 21(4):295–306.
75 Strömberg CA (2011) Evolution of grasses and grassland ecosystems. *Annu Rev Earth Planet Sci* 39:517–544.
76 Morley R, Richards K (1993) Gramineae cuticle: A key indicator of Late Cenozoic climatic change in the Niger Delta. *Rev Palaeobot Palynol* 77(1):119–127.
77 Lister AM (2013) The role of behaviour in adaptive morphological evolution of African proboscideans. *Nature* 500(7462):331–334.
78 Harris JM (1975) Evolution of feeding mechanisms in the family Deinotheriidae (Mammalia: Proboscidea). *Zool J Linn Soc* 56(4):331–362.
79 Sanders W, Gheerbrant E, Harris J, Saegusa H, Delmer C (2010) Proboscidea. *Cenozoic Mammals of Africa*, eds Werdelin L, Sanders WJ (Univ Calif Press, Berkeley, CA), pp 161–251.
80 Laws RM (1970) Elephants as agents of habitat and landscape change in East Africa. *Oikos* 2(1):1–15.
81 Bi X, Sheng G, Liu X, Li C, Fu J (2005) Molecular and carbon and hydrogen isotopic composition of *n*-alkanes in plant leaf waxes. *Org Geochem* 36(10):1405–1417.
82 Whitmarsh RB, et al. (1974) *Initial Reports of the Deep Sea Drilling Project* (US Gov Print Off, Washington, DC), pp 667–752.
83 Wilson KE, et al. (2014) East African lake evidence for Pliocene millennial-scale climate variability. *Geology* 42(11):955–958.
84 Dahl KA, et al. (2005) Terrigenous plant wax inputs to the Arabian Sea: Implications for the reconstruction of winds associated with the Indian Monsoon. *Geochim Cosmochim Acta* 69(10):2547–2558.
85 Huang Y, Clemens SC, Liu W, Wang Y, Prell WL (2007) Large-scale hydrological change drove the late Miocene C_4 plant expansion in the Himalayan foreland and Arabian Peninsula. *Geology* 35(6):531–534.
86 Kingston JD (1999) Isotopes and environments of the Baynunal Formation, Emirate of Abu Dhabi, United Arab Emirates. *Fossil Vertebrates of Arabia*, eds Whybrow PJ, Hill A (Yale Univ Press, New Haven, CT), pp 354–372.
87 Chikaraishi Y, Naraoka H (2006) Carbon and hydrogen isotope variation of plant biomarkers in a plant–soil system. *Chem Geol* 231(3):190–202.
88 Levin NE (2013) *Compilation of East Africa Soil Carbonate Stable Isotope Data*, ed Levin NE (Interdiscip Earth Data Alliance, Palisades, NY).
89 Lüdecke T, et al. (2016) Persistent C_3 vegetation accompanied Plio-Pleistocene hominin evolution in the Malawi Rift (Chiwondo Beds, Malawi). *J Hum Evol* 90:163–175.
90 Cerling T, Harris J, Leakey M (2003) Isotope paleoecology of the Nawata and Nachukui Formations at Lothagam, Turkana Basin, Kenya. *Lothagam: The Dawn of Humanity in Eastern Africa*, eds Leakey MG, Harris JM (Columbia Univ Press, New York), pp 605–623.
91 White TD, et al. (2009) Macrovertebrate paleontology and the Pliocene habitat of *Ardipithecus ramidus*. *Science* 326(5949):67–93.
92 Cerling TE, et al. (2011) Diet of *Paranthropus boisei* in the early Pleistocene of East Africa. *Proc Natl Acad Sci USA* 108(23):9337–9341.
93 Lee-Thorp J, et al. (2012) Isotopic evidence for an early shift to C_4 resources by Pliocene hominins in Chad. *Proc Natl Acad Sci USA* 109(50):20369–20372.
94 Wynn JG, et al. (2013) Diet of *Australopithecus afarensis* from the Pliocene Hadar Formation, Ethiopia. *Proc Natl Acad Sci USA* 110(26):10495–10500.
95 Cerling TE, et al. (2013) Stable isotope-based diet reconstructions of Turkana Basin hominins. *Proc Natl Acad Sci USA* 110(26):10501–10506.
96 Levin NE, Haile-Selassie Y, Frost SR, Saylor BZ (2015) Dietary change among hominins and cercopithecids in Ethiopia during the early Pliocene. *Proc Natl Acad Sci USA* 112(40):12304–12309.
97 Lee-Thorp JA, Sponheimer M, Passey BH, de Ruiter DJ, Cerling TE (2010) Stable isotopes in fossil hominin tooth enamel suggest a fundamental dietary shift in the Pliocene. *Philos Trans R Soc Lond B Biol Sci* 365(1556):3389–3396.
98 Ungar PS, Krueger KL, Blumenschine RJ, Njau J, Scott RS (2012) Dental microwear texture analysis of hominins recovered by the Olduvai Landscape Paleoanthropology Project, 1995–2007. *J Hum Evol* 63(2):429–437.
99 Latorre C, Quade J, McIntosh WC (1997) The expansion of C_4 grasses and global change in the late Miocene: Stable isotope evidence from the Americas. *Earth Planet Sci Lett* 146(1-2):83–96.
100 Yamamoto S, Sawada K, Nakamura H, Kobayashi M, Kawamura K (2014) Stable carbon isotopic variation of long chain *n*-alkanoic acids in the equatorial Pacific sediments over the last 40 Ma: Implications for expansion of C_4 grassland in South America. *Org Geochem* 76:62–71.
101 Hynek SA, et al. (2012) Small mammal carbon isotope ecology across the Miocene–Pliocene boundary, northwestern Argentina. *Earth Planet Sci Lett* 321:177–188.
102 Hoetzel S, Dupont L, Schefuß E, Rommerskirchen F, Wefer G (2013) The role of fire in Miocene to Pliocene C_4 grassland and ecosystem evolution. *Nat Geosci* 6(12):1027–1030.
103 Dupont LM, Rommerskirchen F, Mollenhauer G, Schefuß E (2013) Miocene to Pliocene changes in South African hydrology and vegetation in relation to the expansion of C_4 plants. *Earth Planet Sci Lett* 375:408–417.
104 Passey B, et al. (2009) Strengthened East Asian summer monsoons during a period of high-latitude warmth? Isotopic evidence from Mio-Pliocene fossil mammals and soil carbonates from northern China. *Earth Planet Sci Lett* 277(3-4):443–452.
105 Wang Y, Deng T (2005) A 25 m.y. isotopic record of paleodiet and environmental change from fossil mammals and paleosols from the NE margin of the Tibetan Plateau. *Earth Planet Sci Lett* 236(1-2):322–338.
106 Quade J, Solounias N, Cerling TE (1994) Stable isotopic evidence from Paleosol carbonates and fossil teeth in Greece for forest or woodlands over the past 11 Ma. *Palaeogeogr Palaeoclimatol Palaeoecol* 108(1-2):41–53.
107 Dettman DL, et al. (2001) Seasonal stable isotope evidence for a strong Asian monsoon throughout the past 10.7 my. *Geology* 29(1):31–34.
108 Bond WJ, Keeley JE (2005) Fire as a global 'herbivore': The ecology and evolution of flammable ecosystems. *Trends Ecol Evol* 20(7):387–394.
109 Sankaran M, et al. (2005) Determinants of woody cover in African savannas. *Nature* 438(7069):846–849.
110 Osborne CP (2008) Atmosphere, ecology and evolution: What drove the Miocene expansion of C_4 grasslands? *J Ecol* 96(1):35–45.
111 Polissar PJ, D'Andrea WJ (2014) Uncertainty in paleohydrologic reconstructions from molecular δD values. *Geochim Cosmochim Acta* 129:146–156.
112 Ryan WB, et al. (2009) Global multi-resolution topography synthesis. *Geochem Geophys Geosyst* 10(3):Q03014.
113 Harrison T (2010) Dendropithecoidea, Proconsuloidea, and Hominoidea. *Cenozoic Mammals of Africa*, eds Werdelin L, Sanders WJ (Univ Calif Press, Berkeley, CA), pp 429–469.
114 Wood B, Leakey M (2011) The Omo-Turkana Basin fossil hominins and their contribution to our understanding of human evolution in Africa. *Evol Anthropol* 20(6):264–292.
115 Brown FH, McDougall I, Gathogo PN (2013) Age ranges of Australopithecus species, Kenya, Ethiopia, and Tanzania. *The Paleobiology of Australopithecus*, eds Reed K, Fleagle JG, Leakey R (Springer, New York), pp 7–20.
116 Katoh S, et al. (2016) New geological and palaeontological age constraint for the gorilla-human lineage split. *Nature* 530(7589):215–218.
117 Roth P (1974) Calcareous nannofossils from the northwestern Indian Ocean, Leg 24, Deep Sea Drilling Project. *Initial Rep Deep Sea Drill Proj* 24:969–994.
118 Müller C (1974) Calcareous nannoplankton, Leg 25 (Western Indian Ocean). *Initial Rep Deep Sea Drill Proj* 25:579–633.
119 Fisher RL, et al. (1974) *Initial Reports of the Deep Sea Drilling Project* (US Gov Print Off, Washington, DC), pp 127–196, 283–326.
120 Simpson ESW, et al. (1974) *Initial Reports of the Deep Sea Drilling Project* (US Gov Print Off, Washington, DC), pp 87–138.
121 Marzi R, Torkelson B, Olson R (1993) A revised carbon preference index. *Org Geochem* 20(8):1303–1306.
122 Bush RT, McInerney FA (2013) Leaf wax *n*-alkane distributions in and across modern plants: Implications for paleoecology and chemotaxonomy. *Geochim Cosmochim Acta* 117:161–179.

Supporting Information

Uno et al. 10.1073/pnas.1521267113

SI Materials and Methods

DSDP Marine Core Age Models. Age–depth models were developed for the four DSDP cores using calcareous nannofossil occurrence data (117, 118) and volcanic ashes (60) documented in the cores. We used updated calcareous nannofossil biozonations for the Neogene and the ages assigned therein, which primarily derive from astronomically tuned cyclostratigraphy (61, 62). Biozonations come from top (T) or bottom (B) horizons in the cores. Miocene biozones have an average age uncertainty of ± 0.02 My, whereas, for the Plio-Pleistocene, it is ± 0.007 My. Data are presented in Dataset S1 and Fig. S1.

DSDP Marine Core Sample Description and Age. Marine core sediment samples were taken by the curatorial staff at the International Ocean Discovery Program's Kochi Core Center in Shikoku, Japan. Samples were taken from undisturbed sections of the core where possible. Site and core information are provided in Dataset S3, along with sample locations, calculated depths, and lithological descriptions. Lithological descriptions are condensed from Initial Reports of the DSDP (82, 119, 120). Sample ages were calculated using sample depth to linearly interpolate an age based on adjacent biohorizons in the age–depth models developed at each site (Dataset S1 and Fig. S1). The minimum age uncertainty for each sample is equal to the uncertainty of the associated biohorizon, with uncertainty increasing with sample distance from a biohorizon. The maximum age uncertainty can be estimated as half of the total time represented in the biozone to which the sample belongs. Interpolated ages are presented in Dataset S1.

Biomarker Extraction and Preparation. The outer surface of sediment samples was cleaned with a Dremel to remove possible modern contamination, including drilling mud, which was visually easy to differentiate from sediment, based on color. Samples were lyophilized overnight (−70 °C, ∼10 millitorr) to remove water from sediments. Samples were then solvent-rinsed with dichloromethane (DCM), placed in a mortar and pestle, and crushed to a powder. Between samples, the mortars and pestles were washed, rinsed with deionized water, and solvent-rinsed with methanol and DCM.

Lipids were extracted from 9.1 g to 57.9 g (median: 35.1 g) of powdered samples with organic solvents (9:1 DCM:methanol) using a Dionex Accelerated Solvent Extractor (ASE) 350 packed into 60-mL extraction cells. We found that samples required four 10-min static cycles at 100 °C with a flush volume of 150% to completely extract soluble lipids. An internal standard was added to the ASE extract (2,000 ng of 5α-androstane) for later quantification of lipids.

The total lipid extract (TLE) was transferred to 4-mL vials, and four pilot samples were separated by solid-phase extraction on silica gel columns (∼0.5 g solvent-rinsed silica gel, 230–400 mesh) and analyzed on a gas chromatograph (GC; details in the following section, *Biomarker GC Mass Spectrometry and Isotopic Analyses*) to check for the presence of sulfur and unsaturated compounds in the aliphatic fraction, which contained the *n*-alkanes. Sulfur is common in anoxic sediments and interferes with compounds during measurement on a GC. Both sulfur and minor amounts of unsaturated compounds were present in the aliphatic fraction, necessitating additional sample purification detailed in the following two paragraphs.

TLEs were separated by solid-phase extraction on silica gel columns. The aliphatic fraction (F1) was eluted with 4 mL of hexane, the ketone and ester fraction (F2) was eluted with 4 mL of DCM, and the polar fraction (F3) was eluted with 4 mL of methanol.

To remove sulfur, TLEs were treated with copper. Oxidation of copper to copper sulfide removes sulfur from the sample. DCM- and hexane-rinsed copper wool was added to each F1. Samples were then placed in a thermowell at 50 °C and reacted overnight. The following day, the copper-treated F1 (F1Cu) fractions were loaded directly onto silver ion-impregnated silica get columns (Ag-ion Si gel) in hexane to separate saturated and unsaturated aliphatic compounds. The saturated fraction (F1Cu_S) was eluted in a total of 4 mL hexane, followed by elution of the unsaturated fraction (F1Cu_US) with 4 mL ethyl acetate. Ag-ion Si gel column chromatography was done under low light conditions (columns were shrouded in aluminum foil in a hood with room lights off) to avoid oxidative conditions in the columns.

Biomarker GC Mass Spectrometry and Isotopic Analyses. The *n*-alkanes in the saturated, aliphatic fraction (F1Cu_S) were quantified and characterized on an Agilent GC (Agilent 7890A GC) equipped with both a mass selective detector (5975C MSD) and flame ionization detector (FID). One microliter of sample dissolved in 100 μL hexane was injected into a multimode inlet injector at 60 °C (0.1 min hold) which was then ramped to 320 °C at 900 °C/min and held for the duration of the analysis. Initial GC oven temperature was set at 60 °C (1.5 min hold) and ramped to 150 °C at 15 °C/min, then to 320 °C at 4 °C/min. A helium-purged microfluidics device downstream of a DB-5 column (30 m length, 250 μm i.d.) quantitatively split the GC flow to the MSD and FID detectors. Compound identification was done with comparison of mass spectra and retention times to authentic standards, and *n*-alkane quantification was done by peak integration on the mass 57 ion from the MSD. The *n*-alkane concentrations were calculated based upon the peak area of internal standard of known concentration added to the TLE. We correct for mass-dependent changes in ionization efficiency (or response) using the standard mixture of C_8–C_{40} *n*-alkanes. The response factor correction results in more accurate concentrations of long-chain alkanes.

Carbon isotope ratios of *n*-alkanes were analyzed using a Trace Ultra GC coupled to a Thermo Delta V isotope ratio mass spectrometer through a combustion interface (Thermo IsoLink) at the Lamont-Doherty Earth Observatory Stable Isotope Lab. All sample injections (1–4 μL) were interspersed with injections of molecular mixtures with known isotopic values (Mixes A4, A5, and F8 supplied by Arndt Schimmelmann, Indiana University, Bloomington, IN) that were used for correction of carbon isotope values. The carbon isotope ratio is expressed using delta notation, where $\delta^{13}C = (R_{sample}/R_{standard} - 1)$ and $R = {}^{13}C/{}^{12}C$. We report the $\delta^{13}C$ values of odd-numbered *n*-alkanes C_{27} to C_{35}, where uncertainties for these values incorporate both analytical uncertainty and the uncertainty in converting from the laboratory reference gas scale to the Vienna Pee Dee Belemnite (VPDB) scale (Dataset S5) (111).

ACL and CPI. Terrestrial plant wax molecular distributions are commonly characterized by two metrics, the abundance weighted average chain length (ACL) and carbon preference index (CPI). ACL is calculated as $\sum_{i=a}^{b} iC_i / \sum_{i=a}^{b} C_i$, where C_i is the concentration of the molecule with chain length i (i= 29, 31, 33, 35). The range of ACLs is 29.6–31.5 (Dataset S4).

n-alkanes show a characteristic odd-over-even preference resulting from their biosynthetic pathway. This preference is formalized and calculated, using the CPI (121), as $[C_{27} + 2(C_{29} + C_{31} + C_{33}) + C_{35}]/2(C_{28} + C_{30} + C_{32} + C_{34})$ for *n*-alkanes. CPI values in plants have a wide range (∼0.04–99), although most yield CPIs > 2 (122). The range of CPIs in these samples was 3.5–11.0 (Dataset S4).

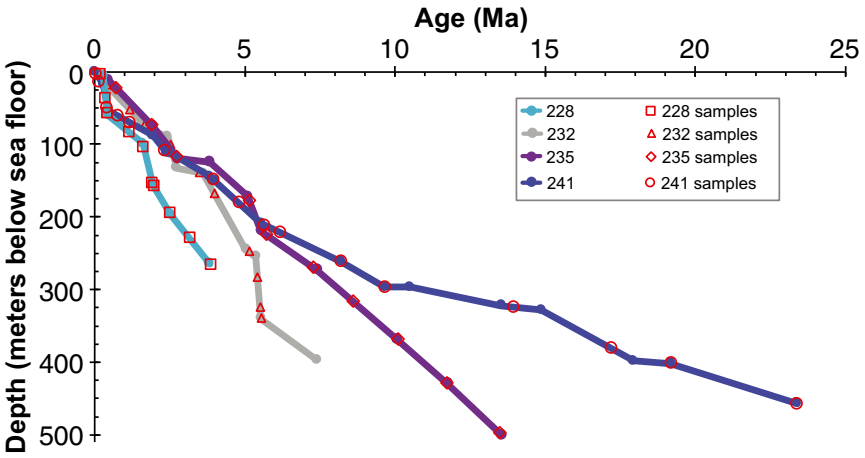

Fig. S1. Age–depth models for DSDP cores are based on calcareous nannofossil biohorizons (61, 62) and volcanic ashes in the cores (3), where each filled circle represents an age–depth tie point. Age uncertainties for tie points are, on average, less than 0.02 My. Biomarker samples are shown with open red symbols.

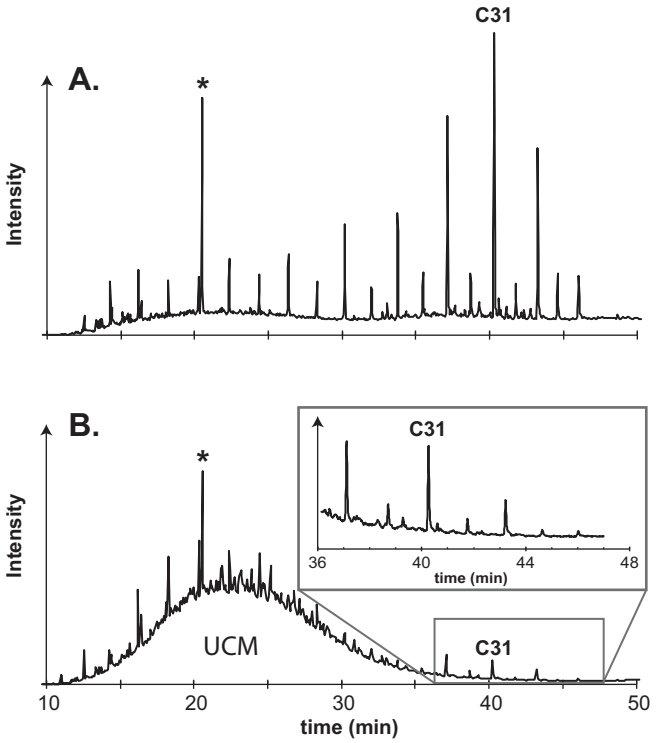

Fig. S2. Gas chromatograms of the saturated aliphatic fractions showing FID detector intensity vs. time. Plant-derived *n*-alkanes used in this study include the C_{27} to C_{35} homologs. The asterisk (*) indicates the internal standard peak (5α-androstane). (*A*) Sample KU354 (Site 241, 9.65 Ma) is representative of most samples analyzed, with characteristic odd-over-even preference in long-chain alkanes. (*B*) Sample KU358 (Site 241, 23.4 Ma) is characterized by a relatively large UCM from 10 min to 35 min. Plant-derived *n*-alkanes elute after the UCM and, although comparatively small, still exhibit characteristic odd-over-even preference and concentrations sufficient to make carbon isotope measurements.

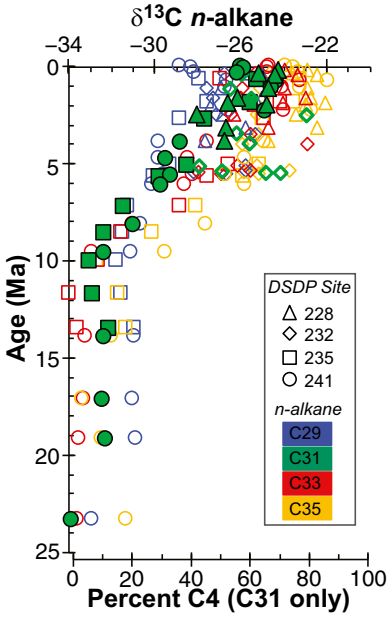

Fig. S3. Carbon isotope data from *n*-C_{29}, *n*-C_{31}, *n*-C_{33}, and *n*-C_{35} alkanes from all four DSDP Sites (228, 232, 235, and 241). Sites are indicated by symbol, and *n*-alkanes are indicated by color.

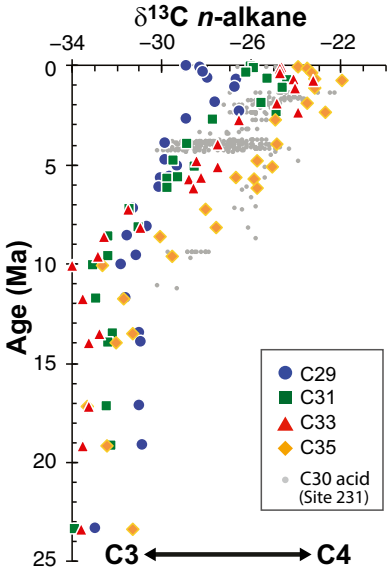

Fig. S4. Carbon isotope data from *n*-C_{29}, *n*-C_{31}, *n*-C_{33}, and *n*-C_{35} alkanes from the Somali Basin DSDP Sites 235 and 241. From 24 Ma to 10 Ma, all $\delta^{13}C$ values correspond to C_3 ecosystems. At 10 Ma, all $\delta^{13}C$ values begin to shift toward more positive values, most pronounced in the +3.1‰ shift in the *n*-C_{35} alkane, signaling the onset of expansion of C_4 vegetation. Also shown are the *n*-alkanoic acid $\delta^{13}C$ values from DSDP Site 231 in the Gulf of Aden (7). These samples also indicate the onset of C4 expansion at ~10 Ma, although the trend and absolute values are different from the Somali Basin sites.

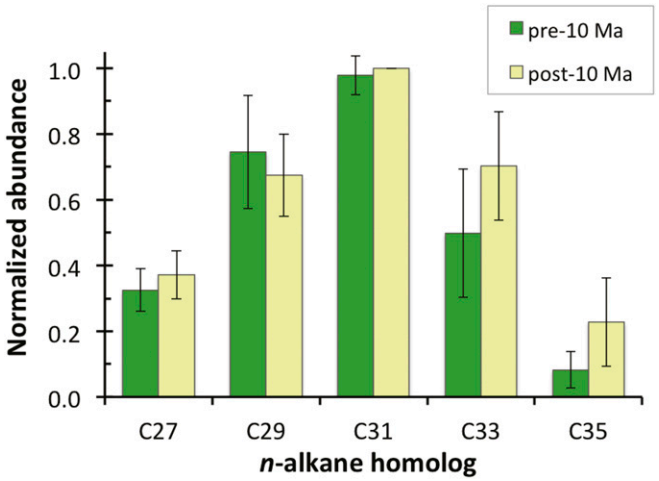

Fig. S5. Molecular distributions of long-chain alkanes from Somali Basin samples divided into two groups, pre- and post-10 Ma. Fractional abundances are normalized to the most abundant homolog (C_{31}) for both groups. The fractional increases in C_{33} and C_{35} and corresponding decrease in C_{29} in post-10-Ma samples with respect to pre-10 Ma supports the isotopic evidence for C_4 grasses and the $\delta^{13}C$ of the C_{35} homolog as a first indicator for the onset of C_4 vegetation expansion. In pre-10-Ma samples, the second most abundant homolog is C_{29} (75% of C_{31}) followed by C_{33} (50%). C_{35} abundance is only 8% of C_{31}. In post-10-Ma samples, C_{33} is the second most abundant homolog (70% of C_{31}), C_{29} is slightly less abundant (67%), and C_{35} increases to 23% of C_{31}.

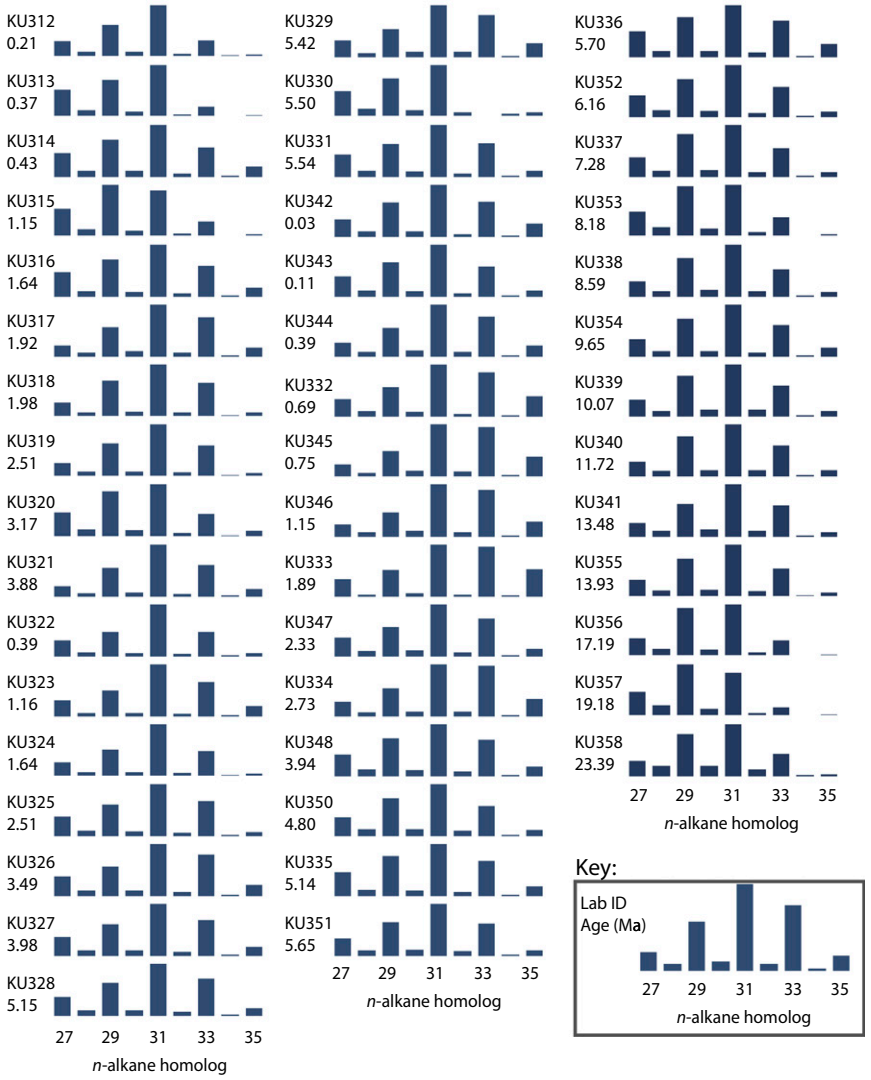

Fig. S6. Normalized molecular distributions for all samples. For concentration and additional sample information, see Dataset S4.

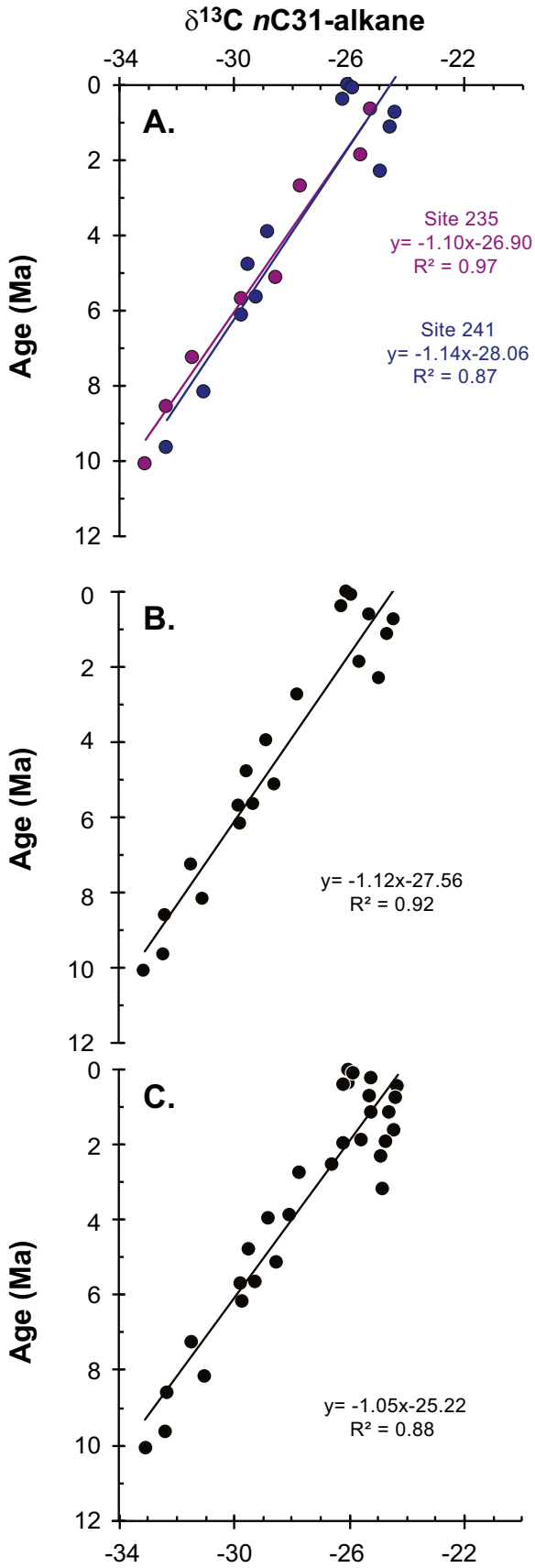

Fig. S7. Linear regressions of $\delta^{13}C$ versus sample age from 10 Ma to present for (*A*) Sites 235 and 241, (*B*) the stack of Somali Basin sites, and (*C*) all sites except for 232, which has been excluded from all Africa data.

Other Supporting Information Files

Dataset S1 (XLSX)
Dataset S2 (XLSX)
Dataset S3 (XLSX)
Dataset S4 (XLSX)
Dataset S5 (XLSX)
Dataset S6 (XLSX)
Dataset S7 (XLSX)